

# Electric Subsystem Model of a Hybrid-Electric Powertrain for a Fixed-Wing Drone<sup>★</sup>

Manuel A. Rendón<sup>\*</sup> Gilberto Buffara<sup>\*\*</sup> Daniel M. Esther<sup>\*\*\*</sup>  
Camila de Oliveira Cunha<sup>\*\*\*\*</sup>

<sup>\*</sup> *Universidade Federal de Juiz de Fora (UFJF), Juiz de Fora, MG,  
(e-mail: manuel.rendon@ufjf.br)*

<sup>\*\*</sup> *Stella Tecnologia, Rio de Janeiro, RJ, (e-mail: buffara@gmail.com)*

<sup>\*\*\*</sup> *Universidade Federal de Juiz de Fora (UFJF), Juiz de Fora, MG,  
(e-mail: daniel.miranda@engenharia.ufjf.br)*

<sup>\*\*\*\*</sup> *Universidade Federal de Juiz de Fora (UFJF), Juiz de Fora, MG,  
(e-mail: cunha.camila@engenharia.ufjf.br)*

---

**Abstract:** The study of hybrid-electric aircraft in recent years was motivated by efforts for diminishing the emissions on aerial transportation. Alternative aircraft powertrain design developments aim for replacing actual technologies, employing several approaches and methodologies. However, to set the basic specifications of a powertrain is a complex challenge. Present work depicts the detailed design and modeling of the electrical subsystem of a hybrid-electric powertrain in serial topology, intended to replace the actual system on a fixed-wing drone from a Brazilian company. The required power and weight of the modeled components were defined on a previous work that analyzes the complete aircraft powertrain and its subsystems. The application that includes electric generator (EG), power electronic converters (PECs), battery pack, and electric motor (EM), was developed in *MATLAB*<sup>®</sup>/*Simulink*<sup>®</sup>. Several power conditions were tested, ranging from zero to nominal power of the set, and with the model submitted to step power variations the electrical variables were sampled. The results in steady state yield the equations that represent the relations of power and efficiency between the input and output of each device. These equations will be applied in a more in-depth analysis for the aircraft studied.

*Keywords:* hybrid-electric powertrain; power electronic converters; aircraft propulsion.

---

## 1. INTRODUCTION

The aviation sector contributes with 2% of the total emissions in world transportation, and is expected to increase up to 11% in the next years (Bravo et al., 2021). Numerous research efforts are focused on developing alternative aircraft powertrain systems. Hybrid-electric propulsion (HEP) is as a highly promising technology with extensive research currently underway. Nonetheless, it faces significant challenges, such as the energy density of storage devices (Sziroczak et al., 2020).

HEP design demands for power systems with specific requirements, and PECs play a crucial role. Published works state the results of using higher voltage levels, complex PEC's architectures, and silicon carbide (SiC) devices. In a published work, a power inverter for a large aircraft claims to improve efficiency and power density. It employs a 3 kV DC bus, much higher than the traditional 270 V, in order to reduce cable mass. The topology is a three-level active neutral point clamped (3L-ANPC) inverter, combining 3.3 kV insulated gate bipolar transistors (IGBTs) with 1.2 kV SiC metal-oxide-silicon field-effect transistors (MOSFETs) (Diao et al., 2023).

Other elaborated PEC structures such as multilevel converters have been tested. A 3 kV active rectifier for a 4 MW aerospace generator drive system was designed with 3-level topology. Its main disadvantage is the increased number of components, with lower power density when compared with simpler methods (Trentin et al., 2021).

Furthermore, a key aspect in HEP PEC systems is the power-to-weight ratio of the battery pack, as well as the discharge C-rate (Finger et al., 2020). Voltage spikes may also be an issue in these devices, which can be addressed through pulse width modulation (PWM) techniques. However, PWM strategies produce large currents, potentially leading to thermal stress-induced damage. A published approach involves the utilization of SiC MOSFETs along with IGBTs to address these challenges (He et al., 2021).

In Richard et al. (2023), an AC electric powertrain was developed without the use of PECs. It provides a direct connection of the EG to one or several permanent magnet synchronous machines (PMSMs), simplifying the architecture and reducing the powertrain weight. However, it causes complex stability issues and non-linearities.

Increasing the speed on EMs augments efficiency and power density, making it advantageous for hybrid applications. However, it yields higher fundamental frequency. Using a “SiC+Si” active-neutral-point-clamped (ANPC)

---

<sup>★</sup> The authors would like to thank the Institutions FAPEMIG and UFJF for supporting actual research, with resources from project N<sup>o</sup> APQ-01421-22, *Edital DEMANDA UNIVERSAL*.

converter allows operation on medium-voltage and high-frequency, reducing voltage spikes (Pan et al., 2021).

Power management in hybrid aircraft is carried out commanding PECs and other subsystems with correspondent control strategies. Batteries are often involved and may be programmed to charge and discharge during flight. The energy stored before flight provides boost power during take-off and climbing. On the cruising phase batteries can be recharged, a DC/DC converter controls the charging current. When using an internal combustion engine (ICE) coupled to a EG as the primary power supply, an AC/DC rectifier is necessary. Optimizing and serving power requirements through different flight stages, the DC/DC converter along with a DC/AC inverter supplies an EM (Miazga et al., 2021).

In Menzi et al. (2024), an ultra-lightweight DC-DC converter for aircraft applications was developed to accomplish optimal power density. The 15 kW system is a Gallium Nitride (GaN) 3-level Buck-Boost converter, achieving a power density of 86 kW/kg, significantly greater than typical values limited on 20 kW/kg.

Present work describes the electrical components model of a hybrid powertrain for a fixed-wing drone. Base parameters were calculated on a previous work (Rendón et al., 2024). The calculated equations of components' efficiencies at part load are shown in the Results section.

## 2. DESCRIPTION OF THE STUDIED AIRCRAFT



Figure 1. *Atobá* fixed-wing drone (MundoGEO, 2022).

*Atobá* is the biggest fixed-wing drone developed in Brazil, classified as a medium-altitude long-endurance (MALE) unmanned aerial vehicle (UAV). It features an autonomy of 28 h with a payload of up to 70 kg, well-suited for a diverse range of tactical and strategic missions (Stella Tecnologia, 2022). It is equipped with *HK S-700E*, a petrol fueled ICE two-cylinder engine, rated at 44.7 kW, mounted on the rear of fuselage, which drives the propeller. More details about *Atobá* and ICE are in Rendón et al. (2024).

Table 1. Electric Subsystem Parameters

Description	Value	Units
Electric Motor Power	24.40	kW
Converters Power	27.01	kW
Battery Power	27.45	kW
Battery Max Energy	32.94	MJ
Battery Power Density	244.00	$\frac{W}{kg}$
Battery Energy Density	292.80	$\frac{kJ}{kg}$
Number of Battery Cells	75.00	-

An application developed in *DieselRK* models the engine in several conditions of altitude above sea level and rotation speed. When operating at 3050 rpm, near its peak efficiency.

The studied aircraft was analyzed on a typical flight mission, with climbing, cruising and descending phases (Rendón et al., 2024). It was modeled with original configuration, and with the hybrid-electric alternative, yielding the parameters disclosed in Table 1.

## 3. HYBRID POWERTRAIN DESCRIPTION

Due to limitations on space inside the aircraft the chosen hybrid-electric topology was series (Figure 2). In this configuration the ICE and propeller are in separated axes, coupled by an electric link, granting ICE operation on its most efficient conditions for the required power. It was set that the ICE in hybrid design driving the EG would be the same engine as in original configuration.

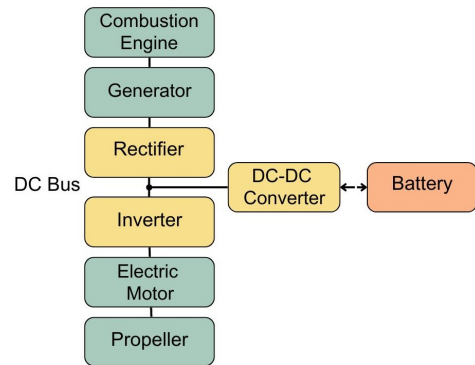


Figure 2. Series Hybrid-Electric Powertrain topology.

The propeller power is supplied by the EM which is empowered from both combustion and battery energy sources. The PEC set with rectifier, bidirectional DC/DC converter and inverter, couples a battery pack as a secondary energy source, which can be either charged or discharged as needed.

### 3.1 Electric Generator / Electric Motor

With the parameters of Table 1 and propeller rotation values along the mission, the machines to be modelled were chosen from existing motors for aircraft applications: *EMRAX 188* for EM, and *EMRAX 228* for EG. Manufacturer information was employed, aiming to operate on high efficiency values during cruise phase, with efficiencies near 96% (EMRAX Innovative E-Motors, 2024). Some of EMs and EGs parameters can be found in Table 2.

Table 2. Information of modeled electric machines (EMRAX Innovative E-Motors, 2024)

Parameter	<i>EMRAX 188</i>	<i>EMRAX 228</i>	Units
Max continuous power	37.0	75.0	kW
Peak power	60.0	124.0	kW
Maximum speed	8000.0	6500.0	rpm
Number of pole pairs	10.0	10.0	-
Internal resistance ( $R_s$ )	5.0	19.0	m $\Omega$
Peak torque	100.0	230.0	N · m
Weight	7.1-7.9	12.9-13.5	kg
Operating voltage	50.0-660	50.0-830	V

### 3.2 Battery Pack

A set of battery cells was modeled with the optimal calculated configuration, 75 cells connected in series with a combined power output  $P_{bat}$  of 27.45 kW (Rendón et al., 2024). The specifications of each battery cell (Winston, 2021) are in Table 3.

Table 3. Battery Parameters

Parameter	Value	Unit
Mass of a cell	1.5	kg
Energy density	292.8	$\frac{\text{kJ}}{\text{kg}}$
Power density	244.0	$\frac{\text{W}}{\text{kg}}$
Nominal voltage of a cell	3.05	V
Battery pack total power ( $P_{bat}$ )	27.45	kW
Battery pack weight ( $m_{bat}$ )	112.5	kg
Battery pack energy ( $E_{batmax}$ )	32.94	MJ
Number of battery cells ( $n_{bat}$ )	75.0	-

### 3.3 Power Electronic Converters: Rectifier/Inverter

A three-leg voltage source converter (VSC) topology was selected for both PECs, with sinusoidal pulse width modulation (SPWM) to achieve low total harmonic distortion (THD). The employed module with six IGBTs of SiC was *SKiiP 39AC12T4V1*, with high switching speeds and low conduction losses. Its characteristics are in Table 4.

Table 4. *SKiiP 39AC12T4V1* (Semikron Danfoss, 2021)

Parameter	Value	Unit
<b>IGBT</b>		
$V_{CES}$ (Saturation Voltage)	1.85 – 2.45	V
$r_{CE}$ (Internal Resistance)	7.0 – 11	m $\Omega$
$R_{th}$ (Thermal Resistance)	0.33	K/W
<b>Diode</b>		
$V_{CES}$ (Forward Voltage)	2.1 – 2.4	V
$r_{CE}$ (Internal Resistance)	5.6 – 8.5	m $\Omega$
$R_{th}$ (Thermal Resistance)	0.52	K/W

### 3.4 DC/DC Bidirectional Converter

A bidirectional DC/DC converter manages the operation of battery pack. Employs the same IGBT module, coupled to filtering inductors in an interleaved topology, aiming to reduce losses, as well as the switching frequencies and ripple. The six IGBTs are employed in three legs with two IGBTs per leg. Each leg alternate the task and operates in either *Buck* or *Boost* mode.

In *Buck* mode, the power flows from the DC bus to the battery, and the charging current is controlled. In *Boost* mode the battery acts as a power source, controlling the discharge current, while the EG and rectifier regulates the DC bus voltage at 670 V.

The Duty Cycle  $D$  for *Buck* and *Boost* modes are in (1) and (2) (Guzmán Santillán, 2021):

$$D_{buck} = \frac{V_{bat}}{V_{DC}} \quad (1)$$

$$D_{boost} = 1 - D_{buck}, \quad (2)$$

$V_{bat}$  is the battery voltage, and  $V_{DC}$  the DC bus voltage.

The inductance of the converter is calculated in (3) (Flores T. et al., 2019):

$$L_{min} = \frac{0.5 \cdot D_{buck} \cdot D_{boost} \cdot V_{DC}^2}{f_s \cdot P_{bat}} \quad (3)$$

where  $f_s$  represents the switching frequency, set on 40 kHz.

The minimum DC-Link capacitance is determined in (4) (Flores T. et al., 2019):

$$C_{DC} = \frac{D}{f_{ripv} \cdot f_s \cdot R} \quad (4)$$

where  $R$  represents the load connected to the DC-DC converter ( $V_{DC}^2/P_{bat}$ ) and  $f_{ripv}$  is the desired ripple factor, set on 0.1.

Finally, the minimum inductor resistance is determined by:

$$R_{min} = \frac{P_{bat}}{C_{DC} \cdot V_{DC}^2} \quad (5)$$

The DC/DC converter's parameters are shown in Table 5.

Table 5. DC/DC Converter Parameters

Parameter	Value	Unit
$V_{DC}$	670.0	V
$V_{bat}$	228.75	V
$f_s$	40.0	kHz
$C_{DC}$	1.0	mF
$L_1, L_2, L_3$	12.554	$\mu\text{H}$
$R_1, R_2, R_3$	76.77	m $\Omega$

## 4. DESCRIPTION OF THE SIMULINK MODEL

An application in *MATLAB*<sup>®</sup>/*Simulink*<sup>®</sup> was developed with three subsections. The first composed by the EG and rectifier, the second includes the DC/DC converter and battery pack, and the third contains the PEC inverter and EM. All of them are connected by the DC bus (Figure 3).

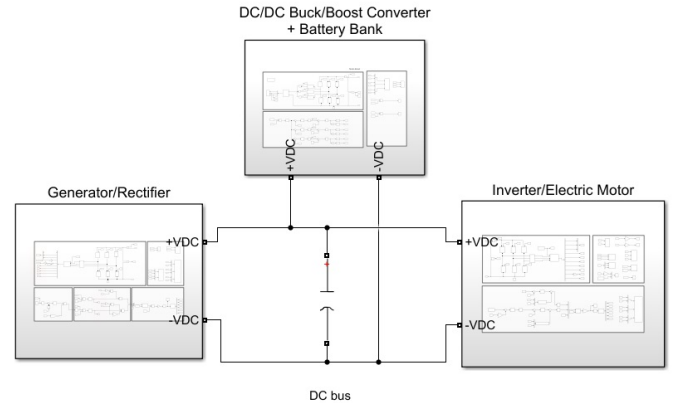


Figure 3. Simulation model in Simulink<sup>®</sup>.

A supervisory control commands the three subsystems. In the climbing phase the propeller power is supplied by the EG and if necessary the battery provides additional power. In cruise phase both PECs the rectifier and DC/DC alternate in power supplying. In descent phase the battery is full-charged and the propeller is driven by the EG.

#### 4.1 Electric Generator and Rectifier

Figure 4 presents the main elements in this subsection. The modeled variable torque represents the ICE actuation.

When the primary power source is the EG, the rectifier control law regulates the DC bus voltage. An inner feedback loop adjust the  $I_q$  current set with a negative reference value. Current control is part of an external feedback loop to control DC bus voltage, where other proportional-integral (PI) compensator is tuned through pole placement (Table 6).

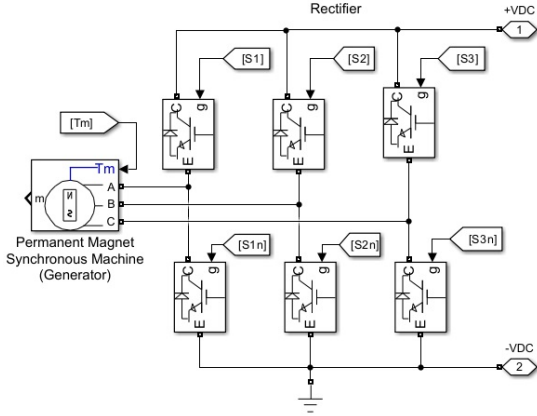


Figure 4. Electric Generator and Rectifier

#### 4.2 DC/DC Converter and Battery Pack

Figure 5 shows the interleaved structure employed for the DC/DC converter, along with the battery.

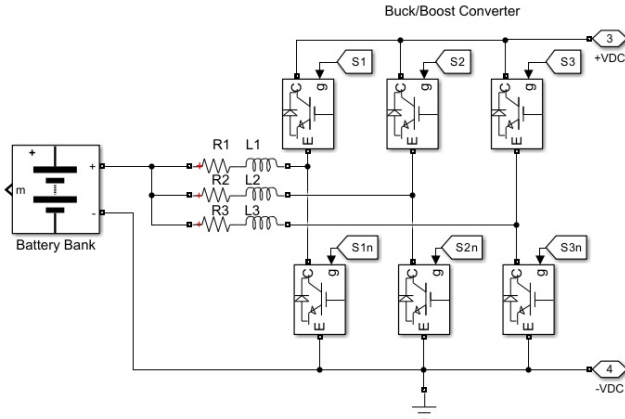


Figure 5. DC/DC Buck/Boost Converter

A battery control law adjusts the charge/discharge current. The small-signal state-space model (Corradini et al., 2015) of the DC/DC converter was obtained. Each leg of the converter can be represented by a first-order transfer function. A PI compensator was employed to control the current. Gain parameters were calculated using pole placement (Table 6).

When the rectifier regulates the DC bus voltage, the DC/DC converter controls the power drawn from the battery pack, set by the reference current. When the propeller is powered by the battery pack, the rectifier is disabled and the DC/DC converter controls the DC bus voltage.

A first-order transfer function correlating capacitor voltage to inductor current was obtained, and superposition was applied to account for each leg; finally, control was achieved with another PI compensator.

#### 4.3 Inverter and Electric Motor

As represented in Figure 6, a model was built for the EM and the IGBT-based VSC. The EM block is tested with a variable input in the load torque ( $T_{load}$ ), that represents the mechanical axis load imposed by the propeller.

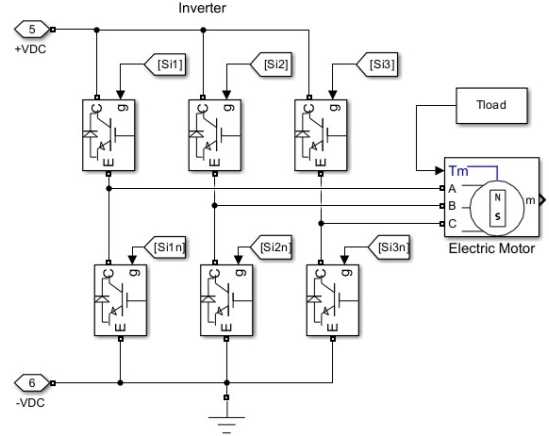


Figure 6. Three-phase Inverter and Electric Motor

The control law regulates the EM speed, simultaneously with the current. A field-oriented control (FOC) was implemented, where the electrical variables are transformed to the time-invariant dq-frame, through the Clarke/Park transformations. In dq-frame, direct-axis and quadrature-axis currents  $I_d$  and  $I_q$ , are controlled with PI compensators in two separated loops, through a decoupling technique using a cascade topology (Figure 7) (Yazdani and Iravani, 2010).

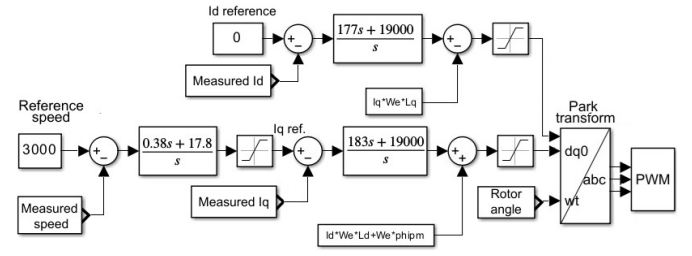


Figure 7. Cascade control

Adjusting  $I_d$  to zero, the maximum induced torque on the EM axis is achieved, and torque becomes directly proportional to  $I_q$ . An external closed loop with a PI compensator controls the shaft speed.

Table 6. PI compensator gains

PEC	Controlled Variable	Gains	
		Kp	Ki
DC/DC converter	Current	-0.000491	-7.17
Rectifier	$V_{dc}$	0.0942	4.4394
Inverter	Speed	0.3768	17.8054
Inverter	$I_d$	177.0	19000.0
Inverter	$I_q$	183.0	19000.0

Control gains were calculated through a pole placement technique, on the second-order transfer function model of the plant. Parameters are shown in Table 6.

## 5. DESCRIPTION OF TESTS PERFORMED AND RESULTS

Tests were conducted varying the power from zero to maximum, aiming to sample electrical variables. In the first configuration the ICE-EG is the power source, with battery and DC/DC converter disconnected. The EM load torque was varied and the inverter control adjusts the power to maintain the EM speed. The power drained from the DC bus is supplied by the rectifier, which control variable is the DC bus voltage.

In the second configuration the battery is the sole power source, with both the EG and rectifier disconnected. The EM load torque was submitted to step variations as in previous, the inverter maintains the speed, while the DC/DC converter controls the DC bus voltage.

In the third configuration the EG charge the batteries, and the EM and inverter are disconnected. Several tests varying the DC/DC converter charging current from zero to maximum were accomplished, while the rectifier control regulates the DC bus voltage.

During the tests torque step variations were applied to the EM, and through FOC, the motor maintained the set point speed of 3000 rpm, while the EG kept the DC bus at 670 V with the action of rectifier control. The performance of some variables after a torque step is shown at Figure 8.

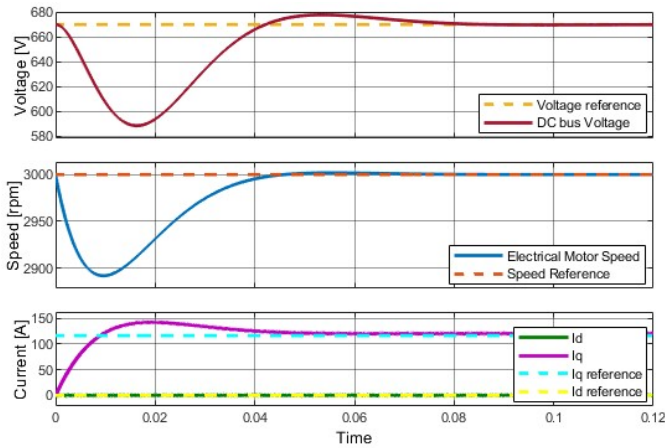


Figure 8. Voltage, Speed and Current control for a 10kW power output

Using the samples in steady state the power at input and output of each set were calculated. The performance was evaluated in the whole range of power for each PEC. The devices' efficiencies were determined as a function of power flow in each set, as observed in Figure 9. As observed the DC/DC efficiency variation with power presents a negative exponential shape.

The relation of efficiencies from EG and EM with power are displayed on Figure 10. The simulated results were plotted next to the experimental data for comparison. Both curves present a negative exponential shape.

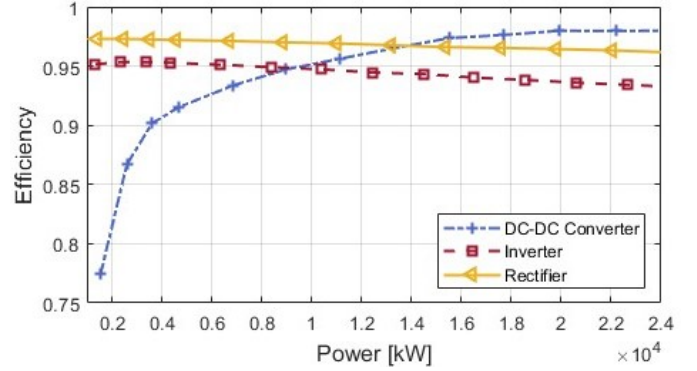


Figure 9. Variation of PEC's efficiencies with Power.

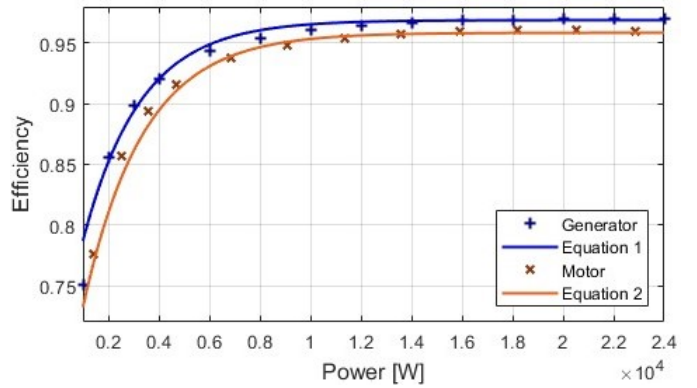


Figure 10. Variation of electric machine's efficiencies with Power.

After obtaining the efficiencies of the individual components, it was possible to calculate the global efficiencies of each subset of PECs, that collaborate in each operation condition of the hybrid motor along the flight mission. Three global efficiencies were then obtained: The first from the output of EG to the inverter output, the second from the output of battery pack to the inverter output, and the third from the rectifier input to DC/DC converter output (Figure 11). As observed efficiency curves show a particular behaviour with power.

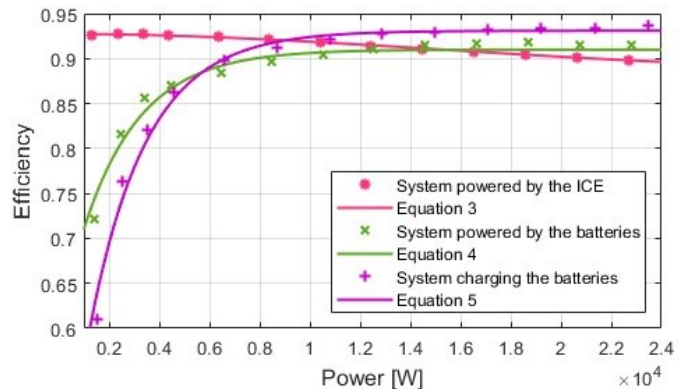


Figure 11. Variation of PECs subsets' efficiencies with Power.

To derive the equations that best describe the negative exponential relation, equations were fitted to the experimental data of EG, EM, and two of three global efficiencies:

$$\eta = A + B \cdot \left(1 - e^{-C \cdot P_{out}}\right), \quad (6)$$

where  $P_{out}$  represents the output power in each case. The equations' parameters can be seen on Table 7, and the adjusted curves (continuous line) are shown with the experimental data (dotted) on Figures 10 and 11.

Table 7. Coefficients of the polynomials

Coefficients	A	B	C
Generator	0.61	0.34	0.00042
Motor	0.69	0.28	0.00044
System powered by Battery Pack	0.60	0.31	0.00044
ICE charging Battery Pack	0.36	0.57	0.00045

The global efficiency of the system when powered by the ICE-EG is described by a 3rd order polynomial equation:

$$\eta = 2.5 \cdot 10^{-15} P_{out}^3 - 1.1 \cdot 10^{-10} P_{out}^2 + 3.5 \cdot 10^{-8} P_{out} + 0.93 \quad (7)$$

## 6. CONCLUSIONS

The calculated steady-state relations of Efficiency vs. Power for subsets of the hybrid-electric powertrain is a valuable tool for studying its influence on the hybrid aircraft performance. Subsets were selected based on the different operation modes of the hybrid engine along the mission.

The calculated values of power and weight for electric machines are corrected with real data from market available products, aiming to study the viability of the proposed hybrid design.

The implementation of SiC IGBTs significantly enhanced the efficiency of the PECs. At an operational point of 10000 W for the EM, the motors achieved peak efficiency, contributing to a well-optimized powertrain. The selected control strategies successfully maintained stability in both the DC bus voltage and motor speed in varying torque demands.

The efficiencies of the powertrain, as a function of power output, were accurately modeled through exponential and polynomial models, providing a reliable basis for predicting fuel consumption across different operational scenarios of a typical flight mission. The nonlinear behavior of the efficiency curves reflects the complex interactions within the powertrain. Present work development may be adapted varying the component's values, or control law strategies to improve the efficiency.

## REFERENCES

- Bravo, G.M., Praliyev, N., and Árpád Veress (2021). Performance analysis of hybrid electric and distributed propulsion system applied on a light aircraft. *Energy*.
- Corradini, L. et al. (2015). *Digital Control of High-Frequency Switched-Mode Power Converters*. IEEE Press.
- Diao, F. et al. (2023). A Megawatt-Scale Si/SiC Hybrid Multilevel Inverter for Electric Aircraft Propulsion Applications. *IEEE Journal of Emerging and Selected Topics in Power Electronics*.
- EMRAX Innovative E-Motors (2024). EMRAX ELECTRIC MOTORS / GENERATORS. URL <https://emrax.com/e-motors/>. Accessed on 05/03/2024.
- Finger, D.F., Braun, C., and Bil, C. (2020). Impact of Battery Performance on the Initial Sizing of Hybrid-Electric General Aviation Aircraft. *Journal of Aerospace Engineering*.
- Flores T., D. et al. (2019). Análisis y diseño de un convertidor Buck-Boost. *La Mecátronica en México*.
- Guzmán Santillán, J.A. (2021). *Diseño y simulación de conjunto convertidor DC-DC e inversor*. Master's thesis, Escuela Superior Politécnica del Litoral (ESPOL).
- He, J., Zhang, D., and Pan, D. (2021). PWM Strategy for MW-Scale "SiC+Si" ANPC Converter in Aircraft Propulsion Applications. *IEEE Transactions on Industry Applications*, 57(3), 3077–3086. doi:10.1109/TIA.2020.3001880.
- Menzi, D. et al. (2024). Ultra-Lightweight High-Efficiency Buck-Boost DC-DC Converters for Future eVTOL Aircraft with Hybrid Power Supply. *IEEE Transactions on Transportation Electrification*.
- Miazga, T., Iwański, G., and Nikoniuk, M. (2021). Energy Conversion System and Control of Fuel-Cell and Battery-Based Hybrid Drive for Light Aircraft. *Energies (Basel)*.
- MundoGEO (2022). Maior drone fabricado no Brasil é exposto ao público pela primeira vez. URL <https://mundogeo.com/2022/01/13/maior-drone-fabricado-no-brasil-sera-exposto-ao-publico-pela-primeira-vez/>. Accessed: 2024-05-01.
- Pan, D. et al. (2021). Control of MW-Scale High-Frequency "SiC+Si" Multilevel ANPC Inverter in Pump-Back Test for Aircraft Hybrid-Electric Propulsion Applications. *IEEE Journal of Emerging and Selected Topics in Power Electronics*, 9(1), 1002–1012. doi:10.1109/JESTPE.2020.2963890.
- Rendón, M.A. et al. (2024). Preliminary Design of Fuel Cell Hybrid-Electric Power-Train for a Fixed-Wing Drone. In *2024 International Conference on Control, Automation and Diagnosis (ICCAD'24)*. IFAC.
- Richard, A. et al. (2023). AC Electric Powertrain without Power Electronics for Future Hybrid Electric Aircrafts: Architecture, Design and Stability Analysis. *Applied Sciences*. doi:10.3390/app13010672.
- Semikron Danfoss (2021). SKiP 37NAB12T4V1 Datasheet. URL <https://www.semikron-danfoss.com/service-support/downloads/detail/semikron-datasheet-skiip-37nab12t4v1-25231570.html>.
- Stella Tecnologia (2022). Ficha Técnica Atobá. <http://www.stellatecnologia.com/wp-content/uploads/2022/09/Ficha-tecnica-Atoba.pdf>. Accessed in 11/30/2023.
- Sziroczak, D. et al. (2020). Conceptual design of small aircraft with hybrid-electric propulsion systems. *Energy*, 204, 117937.
- Trentin, A. et al. (2021). Research and Realisation of High-Power Medium Voltage Active Rectifier Concepts for Future Hybrid-Electric Aircraft Generation. *IEEE transactions on industrial electronics (1982)*, 68(12).
- Winston (2021). TSWB-LYP40AHA. <https://en.winston-battery.com/?cnxdc/318.html>. Accessed in 08/30/2021.
- Yazdani, A. and Iravani, R. (2010). *Voltage-Sourced Converters in Power Systems*. Wiley Sons, Inc.